jove Journal of Visualized Experiments www.jove.com

Video Article

Microfluidic Imaging Flow Cytometry by Asymmetric-detection Time-stretch Optical Microscopy (ATOM)

Anson H. L. Tang[1], Queenie T. K. Lai[1], Bob M. F. Chung[2], Kelvin C. M. Lee[1], Aaron T. Y. Mok[1], G. K. Yip[1], Anderson H. C. Shum[2], Kenneth K. Y. Wong[1], Kevin K. Tsia[1]

[1]Department of Electrical and Electronic Engineering, The University of Hong Kong

[2]Department of Mechanical Engineering, The University of Hong Kong

Correspondence to: Kevin K. Tsia at tsia@hku.hk

URL: https://www.jove.com/video/55840
DOI: doi:10.3791/55840

Keywords: Engineering, Issue 124, Microscopy, imaging flow cytometry, microfluidic, time-stretch imaging, high-throughput screening, single-cell analysis

Date Published: 6/28/2017

Citation: Tang, A.H., Lai, Q.T., Chung, B.M., Lee, K.C., Mok, A.T., Yip, G.K., Shum, A.H., Wong, K.K., Tsia, K.K. Microfluidic Imaging Flow Cytometry by Asymmetric-detection Time-stretch Optical Microscopy (ATOM). *J. Vis. Exp.* (124), e55840, doi:10.3791/55840 (2017).

Abstract

Scaling the number of measurable parameters, which allows for multidimensional data analysis and thus higher-confidence statistical results, has been the main trend in the advanced development of flow cytometry. Notably, adding high-resolution imaging capabilities allows for the complex morphological analysis of cellular/sub-cellular structures. This is not possible with standard flow cytometers. However, it is valuable for advancing our knowledge of cellular functions and can benefit life science research, clinical diagnostics, and environmental monitoring. Incorporating imaging capabilities into flow cytometry compromises the assay throughput, primarily due to the limitations on speed and sensitivity in the camera technologies. To overcome this speed or throughput challenge facing imaging flow cytometry while preserving the image quality, asymmetric-detection time-stretch optical microscopy (ATOM) has been demonstrated to enable high-contrast, single-cell imaging with sub-cellular resolution, at an imaging throughput as high as 100,000 cells/s. Based on the imaging concept of conventional time-stretch imaging, which relies on all-optical image encoding and retrieval through the use of ultrafast broadband laser pulses, ATOM further advances imaging performance by enhancing the image contrast of unlabeled/unstained cells. This is achieved by accessing the phase-gradient information of the cells, which is spectrally encoded into single-shot broadband pulses. Hence, ATOM is particularly advantageous in high-throughput measurements of single-cell morphology and texture – information indicative of cell types, states, and even functions. Ultimately, this could become a powerful imaging flow cytometry platform for the biophysical phenotyping of cells, complementing the current state-of-the-art biochemical-marker-based cellular assay. This work describes a protocol to establish the key modules of an ATOM system (from optical frontend to data processing and visualization backend), as well as the workflow of imaging flow cytometry based on ATOM, using human cells and micro-algae as the examples.

Video Link

The video component of this article can be found at https://www.jove.com/video/55840/

Introduction

Optical imaging presents a powerful tool and cell-based assay to (almost) non-invasively visualize the detailed spatial distribution of many cellular/subcellular components, thus uncovering a multitude of morphological, biophysical, and biomolecular signatures of cells. However, this ability to extract high-content information from single cells has generally been compromised when an enormous and heterogeneous population of cells had to be investigated. This marks a common trade-off in cell-based assays between measurement throughput and content. A notable example is that adding imaging capability to flow cytometry has resulted in a down-scaling of throughput by at least 1-2 orders of magnitude compared to that of the classical non-imaging flow cytometers. Although it could offer complex morphological single-cell analysis that is not possible with standard flow cytometers[1], imaging flow cytometry generally lacks sufficient throughput to identify cellular heterogeneity with high statistical confidence. This is necessary for new discoveries in biology and for gaining an understanding of the pathogenesis of diseases. The key technical challenge lies in the inherent speed limit imposed by the common optical imaging strategies: laser-beam scanning, (*e.g.,* by galvanometric mirrors), and/or image sensors (*e.g.,* charge-coupled device (CCD) and complementary metal-oxide semiconductor (CMOS)). The laser scanning speed is intrinsically restricted by the mechanical inertia of the scanning mirrors, whereas the frame rate of CCD or CMOS is limited by the fundamental trade-off between imaging speed and sensitivity (*i.e.,* increasing the frame rate leads to reduced signal detection sensitivity, and vice versa).

Based on an all-optical, ultrafast image-encoding mechanism, optical time-stretch imaging has been demonstrated as an attractive platform for high-throughput imaging flow cytometers, without need of the conventional image sensors or mechanical laser scanning[2,3]. Detailed descriptions of the working principle of time-stretch imaging can be found in references[4,5,6,7]. In brief, it consists of two interchangeable mapping steps: (i) spectral encoding (wavelength-space mapping), in which the spatial coordinates of the imaged specimen are mapped to different wavelengths across the spectrum of the light-pulsed beam[8,9], and (ii) a dispersive Fourier transformation (wavelength-time mapping)[9], in which the wavelength components of individual laser pulses are transformed (stretched) via group velocity dispersion (GVD) into temporal

(wavelength-swept) waveforms (**Figure 1**). An important feature of time-stretch imaging is optical amplification, which plays a critical role in combatting the loss of sensitivity due to ultrafast photodetection and GVD loss, thus enhancing the image signal-to-noise ratio (SNR) without being contaminated by the photodetector noise[9]. Since each laser pulse encodes a line-scan of the imaged specimen, which is orthogonal to the unidirectional flow of the cells, an effective line-scan rate is determined by the laser repetition rate, which is typically beyond 10 MHz. This ultrafast operation enables blur-free, single-cell image capture at a throughput of 10,000-100,000 cells/s (*i.e.,* 10-100 times higher than conventional imaging flow cytometry). As a result, time-stretch imaging could find unique applications in high-throughput, single-cell, image-based screening, especially when there is a need for identifying unknown heterogeneity or rare/aberrant cells within a sizable population (thousands to millions of cells), such as rare cancer cell screening[10] or micro-algae classification[11].

Time-stretch imaging predominantly relies on bright-field (BF) image capture, from which the image contrast is generated through light scattering and absorption from the cells[2,3,9,10,11]. Such label-free, single-cell imaging capabilities could bypass the detrimental effects associated with the fluorescent labels, such as cytotoxicity and photobleaching, and yet provide valuable information for single-cell analysis based on the cellular and sub-cellular texture and morphology. These label-free parameters are proven to be effective for the deep image classification of cells, especially when an enormous cell population is available[11,12]. However, in many occasions, BF imaging fails to provide sufficient contrast to reveal the detailed morphology of the label-free transparent cells. Different label-free, phase-contrast, time-stretch imaging modalities have been developed for enhancing the imaging contrast at ultrafast frame rates[13,14,15]. Among these techniques, asymmetric-detection time-stretch optical microscopy (ATOM) was developed to reveal the phase-gradient (differential-interference-contrast-(DIC)-like) contrast based on a concept similar to Schlieren photography, enabling the label-free, high-contrast imaging of single cells at an ultrahigh microfluidic speed (up to 10 m/s)[16]. This effect can be readily generated through oblique detection or illumination by partially blocking the image-encoded beam path or tilting the beam before photodetection. Another advantage of ATOM is its ability to simultaneously acquire two phase-gradient contrasts along opposite orientations. Intensity subtraction and summation of two opposite-contrast images yield the differential phase-gradient contrast and the absorption contrast, respectively, from the same line-scan. This work presents a detailed protocol describing the implementation of ATOM, including the establishment of the optical setup, the sample preparation, and the data acquisition and visualization. Specifically, this work demonstrates the ATOM operation with single-cell imaging of human blood cells, cancer cells, and phytoplankton (microalgae). This highlights the applicability of ATOM to imaging flow cytometry, not only in the biomedical arena, but also in marine and biofuel research[17,18].

Protocol

1. Sample Preparation

1. **Sample preparation (adherent cells; MCF-7 cells)**
    1. Take out the cell culture dish from the incubator and drain the culture medium.
    2. Rinse the cells on a dish with 1x phosphate-buffered saline (PBS) to remove excessive culture medium.
    3. Add 3 mL of a solution of 0.25% trypsin to the culture dish (diameter of 100 mm) and put it in a 37 °C, 5% CO_2 incubator for 4 min.
    NOTE: The trypsin dissolves the adhesive protein of the cells so that they will detach from the culture dish.
    4. Check to see if all the cells have detached from the culture dish using a light microscope (10X objective). If not, gently shake the cell culture dish.
    5. Add 4 mL of the standard culture medium (formulated with 89% Dulbecco's Modified Eagle Medium (DMEM), 10% fetal bovine serum (FBS), and 1% penicillin-streptomycin (PS)) to stop the action of the trypsin.
    6. Transfer the whole mixture (cells in trypsin solution and culture medium) to a centrifuge tube and centrifuge for 5 min at 200 x g.
    7. Remove all the fluid and re-suspend the cells in 1 mL of 1x PBS (pH value: 7.4, pre-heated to 37 °C).

2. **Sample preparation (cultured micro-algae)**
    1. Transfer the cultured micro-algae and the culture medium (*e.g.,* sea water, agar, or fresh water) to new glass culture tubes (~15 mL) in a volume ratio (micro-algae to culture medium) of 1:5 to establish a new sub-culture medium.
    2. Place the glass culture tubes in a dust-proof chamber under constant illumination by artificial lighting from fluorescent bulbs according to a light/dark (LD) cycle (usually LD 16:8) for 72 - 120 h before the experiment.
    3. Transfer the sub-cultured samples to a centrifuge tube and mix well.

2. ATOM System Setup

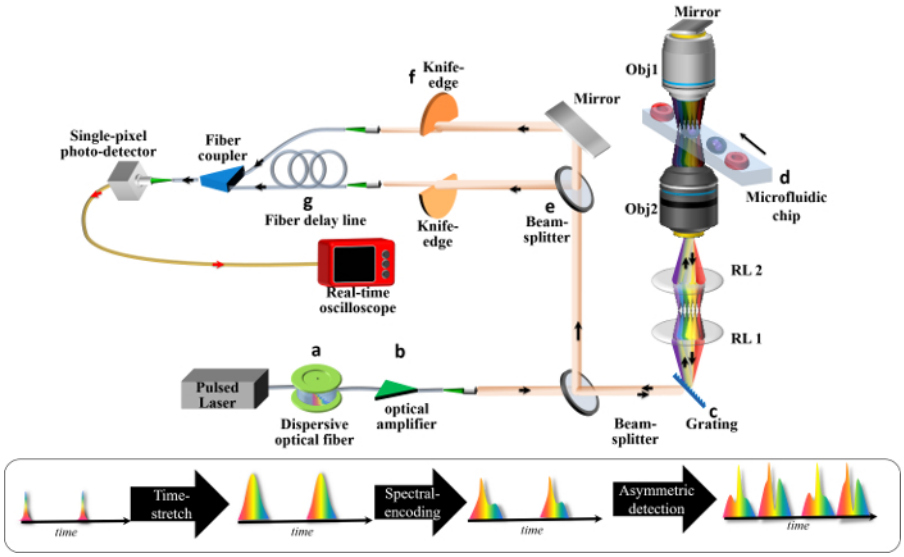

Figure 1: Schematic of an ATOM System. A broadband pulsed laser is employed to deliver ultrafast pulses to (**a**) a time-stretch module and (**b**) an in-line optical amplifier module. The time-stretch module generates a train of temporal waveforms, each of which is the replica of the wavelength spectrum of the laser source, (*i.e.,* wavelength-to-time mapping). The amplifier module is used to for pulse-stretching (dispersive) loss compensation. The stretched pulse is then (**c**) spatially dispersed by a diffraction grating, forming a 1D spectral shower illumination in which individual wavelength components are relayed by a relay lens pair and focused by the objective lens onto different positions on the flowing cell inside the (**d**) microfluidic chip. This is the process of spectral-encoding. The spectrally encoded light will again pass the cell through another objective lens and a mirror, returning to the diffraction grating and recombining as a spatially undispersed pulsed beam. This image-encoded pulsed beam is then (**e**) split into two paths, such that both beams are partially blocked with (**f**) the knife edge, but from opposite directions, before being coupled into the fibers. These two beams represent the two (opposite) encoded phase-gradient contrasts of the final image. For the simultaneous detection of both signal contrasts, one of the signals undergoes (**g**) a time-delay line, such that the two signals are multiplexed (interleaved) in time. A high-speed photodetector and real-time oscilloscope are used for data acquisition. Please click here to view a larger version of this figure.

1. **Time stretch module**
    1. Employ a broadband femtosecond (fs) or picosecond (ps) pulsed laser source with a recommended center wavelength in the near infrared (NIR) range, 800-1,500 nm.
    NOTE: The typical required pulse width can range from sub-100 fs to a few ps. Detailed requirements of the pulsed laser sources can be seen in References 4 and 5. Important metrics are highlighted in **Table 1**.
        1. Ensure that the laser source has a high repetition rate, which should be in the megahertz regime (*e.g.,* tens of MHz) to ensure ultrafast imaging in ATOM. Also, set the peak output laser power well below the damage power threshold of the fiber cavity, approximately 1 kW.
        2. Ensure good shot-to-shot temporal and spectral stability of the pulsed laser source.
        NOTE: Typical tolerance in the spectral amplitude fluctuation should be kept within 1.2%[19,20,21], as achieved by the fiber mode-locked laser in this setup.
        NOTE: The optical bandwidth of the laser source is expected to be 10-100 nm, which is essential to guarantee sufficient imaging field-of-view (FOV) in single-cell imaging[21].

    2. Through a fiber collimator, couple the laser pulsed beam to a single-mode dispersive optical fiber, in which the pulses are stretched via group velocity dispersion (GVD) (**Figure 1a**).
    NOTE: This is the process after which the spectrum of each pulse is mapped onto time as a wavelength-swept waveform (*i.e.,* wavelength-to-time mapping).
    NOTE: The total required GVD should be sufficient to ensure that the overall ATOM image resolution is not affected by the wavelength-to-time mapping process (See the Discussion). Typically, in the NIR range, the GVD should be well beyond 0.1 ns/nm. For instance, a single-mode fiber employed in this current setup provides a total GVD of 0.38 ns/nm around the wavelength of 1,060 nm (a total fiber length of 10 km).

2. **Spectral-encoding module**
    1. Construct an optical microscope system to perform the spectrally encoded imaging of the cells flowing along the microfluidic channel, as illustrated in **Figure 1**.
    NOTE: The key components of this optical microscope include: (1) a diffraction grating, a telescopic relay-lens module (RL1 and RL2 in **Figure 1**), and two objective lenses (Obj1 and Obj2 in **Figure 1**).
        1. First, illuminate the time-stretched and collimated beam onto a diffraction grating (transmission-type grating is employed in this setup) to generate a spectral shower (**Figure 1c**).
        NOTE: The power of the diffracted beam (*i.e.,* diffraction efficiency) can be maximized by adjusting the grating orientation closed to the Littrow configuration.

2. Configure the two relay lenses (RL1 and RL2) in a 4-f imaging system (*i.e.,* place the diffraction grating on the focal plane of RL1 and separate RL1 and RL2 by a distance equal to the sum of their focal lengths. The spectral shower will then be imaged onto the back focal plane of the objective lens Obj1).
3. Carefully align the spectral shower to fill the back aperture of the Obj1, such that the spectral shower can be projected and focused onto the image plane of the microscope.
   NOTE: Here, the NA of the objective lens (Obj1 in **Figure 1**) is 0.75.
4. Place another objective lens (Obj2 in **Figure 1**) with a similar NA and a plane mirror at the back aperture of this objective lens (Obj2), such that the spectral shower beam can be aligned to double-pass the image plane and return to the diffraction grating.
5. Adjust the pair of objective lenses (Obj1 and Obj2) such that their focal planes overlap with each other. Check to see if the spectral shower double-passes the image plane at the same location and returns to the grating following the same path. If not, perform further alignment and tuning of the optical system.
   NOTE: The returned light should pass through an additional beam-splitter, such that the light can be transmitted to an asymmetric detection module.
6. Adjust the optical amplifier gain at a suitable level, such that the resultant signal can be detected by the photodetector with a good SNR, which is typically at >10 dB.
7. Place and adjust the position of the microfluidic chip on the sample platform and make sure that the spectral shower, and thus the imaging area, is placed across the microfluidic channel (**Figure 1d**).
   NOTE: The spectral shower is illuminated orthogonally to the flow direction of fluidics inside the microfluidic chip, such that the flowing motion automatically performs two-dimensional (2D) scans.

3. **Asymmetric detection module**
   1. Place an additional beam-splitter to separate the imaged-encoded beam into two (**Figure 1e**).
      NOTE: Each beam replica is partially blocked by a knife edge.
   2. Measure and record the optical power of the beam before the beam block. Then, manually position the knife edges (mounted on a linear translation stage) such that they roughly block half of the beam (by visual inspection). Afterward, use the optical power meter to monitor the beam power while fine-tuning the position of the knife edges by translating them across the beam.
      NOTE: It is suggested that the optimal position is where the power is decreased by ~50% of the original value (*i.e.,* the unblocked case). This is the condition that provides the best combination of image signal strength and image contrast enhancement.
   3. Repeat step 2.3.2 for another beam replica. Note that the orientation of the partial beam block for one beam should be opposite with respect to the other beam (**Figure 1f**).
   4. Couple the two partially-blocked beams into two separate, single-mode fiber arms through two-fiber collimators.
      NOTE: One of the arms has an extra length of fiber, serving as a fiber-based delay-line, to introduce a time-delay with respect to the other replica (without the delay-line) (**Figure 1g**). Both are directed to a single fiber by a fiber coupler before photodetection. The time-delay should be long enough to temporally separate the two replicas and short enough to avoid temporal overlap with the next waveform (*i.e.,* the two replicas are always time-interleaved and time-multiplexed in a single fiber prior to detection (**Figure 2a**)).
   5. Capture and digitize the detected optical signals with the real-time oscilloscope. Note that the bandwidth and thus the sampling rate of the oscilloscope should be sufficiently high to ensure that they do not influence the final image resolution (See the Discussion).
      NOTE: Here, with the GVD of 0.38 ns/nm, a backend acquisition bandwidth and sampling rate of >20 GHz and >40 GSa/s, respectively, are required.

3. Experimental Procedures

1. **Specimen loading**
   1. Perform cell counting under a conventional phase contrast microscope in a standard hemocytometer.
   2. Adjust the cell density by diluting with 1x PBS (with spring water for micro-algae) and mix well with a pipette.
      NOTE: The suggested concentration is from 10^5 to 10^6 cells/mL.
   3. Mount the microfluidic chip onto the sample platform of the optical imaging system.
      NOTE: The microfluidic chip is primarily made of polydimethylsiloxane (PDMS) and is fabricated using the standard replica molding method. The microfluidic channel is designed with an asymmetric curved channel to generate the inertial flow focusing effect, such that the cells can flow in single file in the imaging section (with a dimension of 80 µm x 80 µm (height x width)) at high speed.
   4. Transfer the density-adjusted cell solution to a 10 mL syringe.
   5. Connect the syringe to the inlet of the microfluidic chip and a centrifugal tube to the outlet of the microfluidic chip for disposal collection.
   6. Mount the syringe onto a syringe pump and set a suitable flow rate to give desirable throughput and to avoid imposing excessive shear force between the cells and the channel.
      NOTE: The linear speed of the samples should be within 0.5 and 10 m/s. Note that before the actual image recording, it is often necessary to further fine-tune the system, in terms of maximizing the image signal strength and optimizing the image focusing by repeating steps 2.2.1.4-2.2.1.6.

4. Data Acquisition

1. Set a suitable number of data points to be saved for each experiment. The number of data points to be saved depends on the size and flow rate of the samples.
   NOTE: Typically, it is set to 8-16 million sample points under a sampling rate of 80 GSa/s.
2. Acquire and save the data in a batch mode using the oscilloscope.

5. Backend Processing

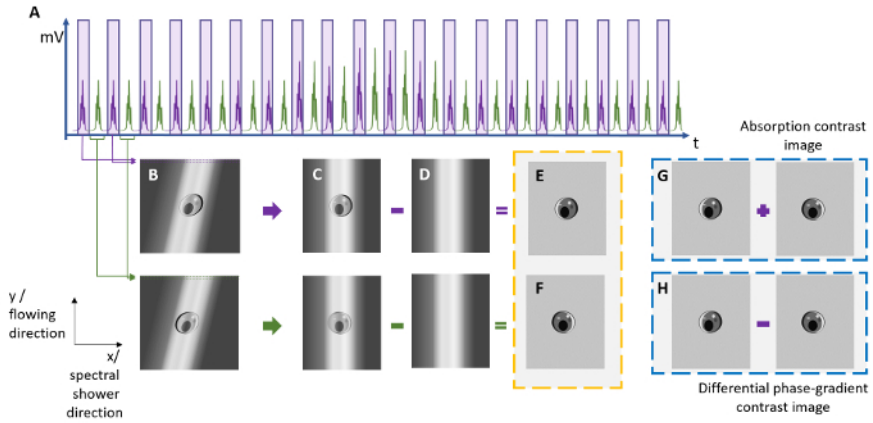

Figure 2: Reconstruction of ATOM Images from the Line-scan Time Trace. To reconstruct the ATOM images with the absorption contrast and differential (enhanced) phase-gradient contrast, two sets of time-stretched pulses (see the purple and green pulses) are extracted from (**a**) the time-multiplexed temporal waveform trace and are then digitally segmented and stacked to form (**b**) two 2D images showing the two opposite phase-gradient contrasts. Note that a shearing operation is needed to form (**c**) the distortion-free images by compensating for the sub-index shift due to the round-off error in the laser repetition rate estimation. By subtracting the (**d**) raw line-scan from the spectral intensity envelope of the laser source, the background of the images can be removed. (**g**) An absorption contrast image can be obtained by a pixel-by-pixel intensity summation of images (**e**) and (**f**), whereas (**h**) a differential phase-gradient contrast image can be obtained from the subtraction of images (e) and (f). Please click here to view a larger version of this figure.

1. **Transfer the data from the oscilloscope to the computers for offline image reconstruction.**
   NOTE: Here, the data are stored in a portable hard disk and transferred manually between the oscilloscope and the processing computers. The capacity of the hard disk should be more than 500 GB for each experiment.
   1. Use the key image reconstruction routine to digitally stack the line-scans to form a 2D image (**Figure 2**).
      NOTE: The custom program (in MATLAB) then produces two asymmetric detection images by separating the two time-multiplexed data sets (purple and green waveforms in **Figure 2**).
      1. Obtain a differential phase-gradient contrast image by subtracting the intensities of the two asymmetric detection images; an absorption contrast image can be obtained by adding the two asymmetric detection images. See selected images of MCF-7 and micro-algae in **Figure 3**. Note that the background profiles of individual images should first be eliminated, and their intensities should be normalized, prior to the image summation and subtraction operations.
   2. Generate a library of parameters derived from the images, such as cell volume, circularity, and absorption density, *etc.* for further analysis.

2. **Input the library of data into the data visualization platform (Figure 4).**
   1. Load the library of parameters and the corresponding reconstructed images to the visualization interface platform.
   2. Set the axes to be the parameters of interest.
      NOTE: The parameters are problem-specific and are defined by the user. They are derived from the ATOM images by the MATLAB program. Here, the optical absorption density of the cell, cell area, cell volume, and cell circularity are available for selection.
   3. Select the dataset to be displayed, such that every cell image can be visualized as a different data point on the scatter plot.
   4. Move the mouse cursor to each point, such that the corresponding image and other parameters are shown in a floating sub-window.
      NOTE: The axes can be changed between the linear and logarithmic scales in an interactive manner.
   5. Perform further analysis of any subset of the dataset by manually gating on the scatter plot.
      NOTE: The histogram in every parameter of the gated subset can be plotted against those of the entire library. The separate histograms are displayed in another floating sub-window.

Representative Results

This work illustrates two single-cell imaging demonstrations by ATOM: one with mammalian cells (human peripheral blood mononuclear cell**s** (PBMC) and breast cancer cells (MCF-7)) and another with phytoplankton**s** (Scenedesmus and Chlamydomonas). The first experiment was motivated by the growing interest in liquid biopsy for the detection, enumeration, and characterization of circulating tumor cells (CTCs) in the blood[23]. The ability to measure CTCs disseminated from primary tumor sites to the blood stream allows for the examination of metastatic cancer progression[24,25]. However, challenges exist in CTC analysis: (i) the CTC count is significantly lower than the exorbitant amount of blood cells in whole blood. Current methods of identifying and recovering the CTCs mostly involve cell enrichment and separation steps[26,27,28]. However, the contaminating background from blood cells and/or the viability of the enriched CTCs remain a concern for subsequent molecular analysis (*e.g.,* RNA sequencing)[29]. (ii) CTCs are highly heterogeneous in terms of both biophysical and biomolecular signatures, limiting the efficiency of the CTC enrichment and detection. To this end, label-free imaging flow cytometry with a high imaging throughput is an appealing tool that allows for the direct imaging and identification of CTCs within an enormous population of blood cells, minimizing or even bypassing the enrichment steps.

The second experiment is particularly relevant to large-scale phytoplankton characterization, which can impact advances in environmental sciences (*e.g.,* the detection of harmful algal bloom (HAB) species[29] and the identification of microalgal species as renewable biodiesel sources)[17]. Enabled by ATOM, the capability of high-throughput and high-contrast single-cell imaging of phytoplankton could be valuable to reveal the complex heterogeneity in size, texture, and morphology across different genus and species.

Figure 3 shows images of mammalian cells, MCF-7 and PBMC (flowing at a speed of ~10 m/s), as well as microalgae, Scenedesmus and Chlamydomonas (flowing at a speed of ~2 m/s), captured by ATOM. In all four cases, the two opposite phase-gradient contrasts were obtained by the two time-multiplexed, asymmetrically detected signals (described in step 2.3). They both exhibit a pseudo-three-dimensional appearance, resembling the DIC images, each of which shows two opposite shadowing orientations (columns 1 and 2 in **Figure 3a-d**). Evaluating the pixel-wise intensity sum and difference of these two opposite-contrast ATOM images, it was possible to simultaneously obtain two additional ATOM contrasts (*i.e.,* the absorption-only and enhanced differential phase-gradient contrasts; columns 3 and 4 in **Figure 3a-d**). Note that not only can label-free ATOM reveal the blur-free single-cell images, but also characterize cellular structures with high contrast. Notably, the vacuoles, pyrenoid, and flagella in the micro-algae can be clearly visualized in **Figure 3**. This imaging attribute critically enables the extraction of a rich set of identifiers derived from the intrinsic cellular and subcellular textures/morphologies for automated image-based classification.

This work demonstrates that biophysical properties, such as cell circularity and cell size, can be used for the classification of MCF-7 and PBMC. Note that two clusters are observed in the MCF-7 specimen. The availability of high-contrast images for all data points allow us to scrutinize that one of the clusters corresponds to fragments/debris (**Figure 4a**). A similar classification between two species of phytoplankton based on ATOM images was also performed. Here, the classification results are presented in a form of a 2D scatter plot visualized by the customized user interface (**Figure 4**). Each annotated data point in the scatter plot, corresponding to each cell, can be further explored with different parameters derived from ATOM. The corresponding ATOM image can also be interactively displayed directly on the plot. Manual gating is also supported in this visualization interface to facilitate further classification and analysis.

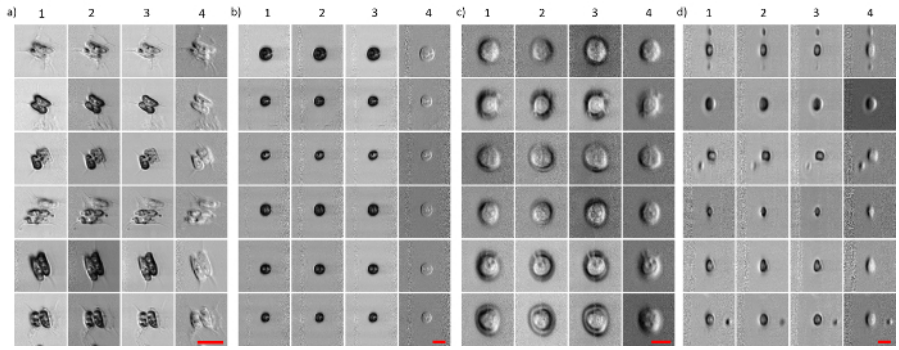

Figure 3: ATOM Image Galley of Micro-algae and Mammalian Cells at an Ultrafast Flowing Speed (~2-10 m/s). (**a**) Scenedesmus; (**b**) Chlamydomonas; (**c**) breast cancer cells, MCF-7; and (**d**) human PBMC. The Scenedesmus and Chlamydomonas are flowed at ~2 m/s, whereas MCF-7 and PBMC are flowed at 10 m/s. The left two columns (columns 1 and 2) for each cell type represent two opposite phase-gradient contrasts. Columns 3 and 4 represent the absorption contrast and differential (enhanced) phase-gradient contrast, respectively. Scale bars = 20 µm (in red). Please click here to view a larger version of this figure.

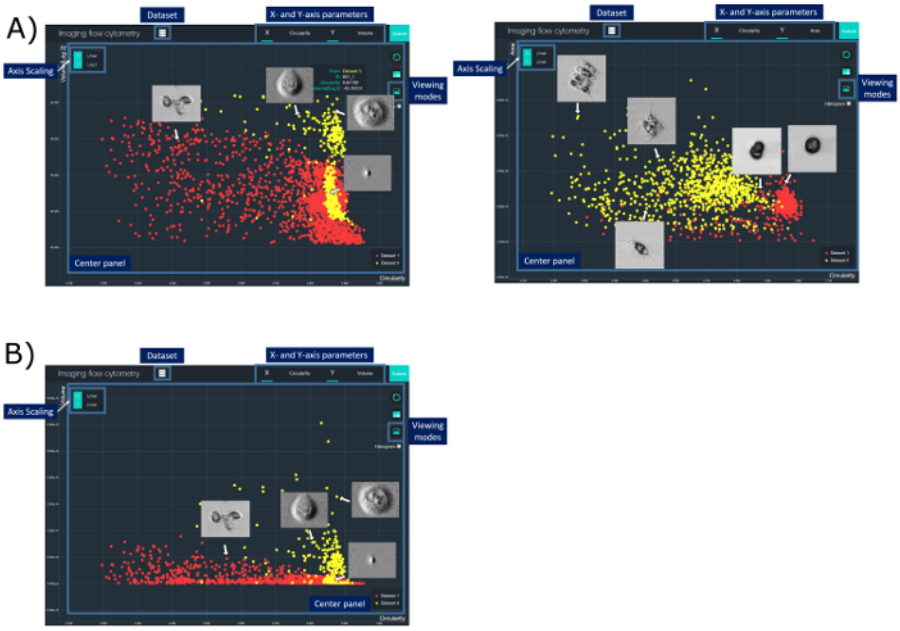

Figure 4: A Graphical User Interface for Cytometric Analysis Based on ATOM Images. In this interface, the user can perform cell-type classification and analysis by defining different cell parameters (*e.g.,* cell size, circularity, absorption density, *etc.*) derived from the ATOM images. The result can be represented in a scatter plot displayed in the center panel. Access and control of various display options, which include changing parameters and scaling for the x- and y-axis (X- and Y-axis parameter buttons) and switching between data sets (Dataset button), is possible. Detailed cell information (Cell information tab) can be read by hovering on a specific data point. To enable rapid navigation, the user can change to another viewing mode and simultaneously display all images on the scatterplot in the center panel (Viewing modes button). Manual gating can also be performed for further analysis. Yellow data points represent the MCF-7 cell specimen (in (**a**)) and Scenedesmus (SCE) (in (**b**)), whereas the red data points represent the human PBMC specimen (in (a)) and Chlamydomonas (CHA) (in (b)). Please click here to view a larger version of this figure.

Discussion

There are several technical details that require special attention during the ATOM system setup. First, it is essential to note that asymmetric/oblique spectrally-encoded illumination could introduce residual phase-gradient components (*i.e.,* the shadowing effect) in the absorption contrast and influence the enhancement of phase-gradient contrast in ATOM. Therefore, this effect of oblique illumination should be minimized. Second, it should be emphasized that the time-multiplexing or time-interleaving schemeinvolving two replicas results in no significant compromise on the imaging speed (*i.e.,* the line-scan rate of >MHz can still be maintained), given that the total temporal width of two beam-replicas does not exceed one line-scan period. Third, the optimal configuration of the integrated module of dispersive fiber and amplifiers depends upon the targeted gain as the specification of the available amplifiers. Optical amplification is essential to the process of time-stretch to combat the optical loss associated with GVD[22]. In principle, it can be implemented by any type of optical amplifier, preferably in the fiber format, such that it is compatible with the fiber-based, time-stretch process (**Figure 1b**). Practical examples of optical fiber-based optical amplifiers include erbium-doped fiber amplifiers (EDFA; for operation wavelengths of ~1,500-1,600 nm), ytterbium-doped fiber amplifiers (YDFA; for operation wavelengths of ~1,060 nm), fiber Raman amplifiers, and fiber optical parametric amplifiers (FOPA; for any operation wavelength, in principle, as long as a pump laser source is available). Amplifier noise must also be carefully considered in the module design. Detailed theory can be seen in Reference 8. A common configuration could involve multiple/cascaded fiber amplifiers inserted between multiple dispersive fiber segments (each has a length of a few km). For ATOM and time-stretch imaging in general, the typical on-off optical power gain should be around 20-30 dB. It should be noted that the operation wavelength range is typically restricted to ~800-1,550 nm, mainly due to the exceedingly high optical fiber loss at shorter wavelengths (*i.e.,* visible wavelengths). Therefore, similarly to the majority of the time-stretch imaging demonstrations, *fiber-based* ATOM will not be immediately applicable to fluorescence imaging where visible-light operations are still commonplace. Nevertheless, note that a *free-space* pulse-stretching concept resembling time-stretch, called free-space angular-chirp-enhanced delay (FACED), has recently been used for ultrafast laser-scanning imaging in ATOM, as well as for fluorescence imaging at visible wavelengths[30].

Another important parameter requiring subtle design consideration is image resolution. Unlike classical light microscopy, the image resolution of ATOM and general time-stretch imaging along the spectral shower axis is governed by three limiting regimes[22]: (i) the spatial-dispersion-limited resolution, which is related to the *spectral* resolution of the diffraction grating, denoted as $\boldsymbol{\delta x}^{spatial}$; (ii) the stationary-phase approximation limit, which is defined as the ambiguity of the wavelength-time mapping process $\boldsymbol{\delta x}^{SPA}$, which inversely scales with the square root of GVD[22]; and (iii) the photodetector-limited resolution $\boldsymbol{\delta x}^{det}$, which describes the finite bandwidth of the photodetector that could also influence the final spatial resolution. In general, the largest value among these three parameters is defined as the image resolution of ATOM, $\boldsymbol{\delta x}$ (*i.e.,* $\boldsymbol{\delta x} = \max\{\boldsymbol{\delta x}^{spatial}, \boldsymbol{\delta x}^{SPA}, \boldsymbol{\delta x}^{det}\}$). It is always desirable to ensure that the final resolution is spatial-dispersion-limited (*i.e.,* $\boldsymbol{\delta x} = \boldsymbol{\delta x}^{spatial} > \boldsymbol{\delta x}^{SPA} > \boldsymbol{\delta x}^{det}$). Therefore, both the GVD (step 2.2.1.1) and the bandwidth (step 2.3.5) of the photodetector must be sufficiently high to satisfy this condition. On the other hand, the image resolution along the flow direction is evaluated by the diffraction limit. This is only true when the Nyquist's sampling condition is satisfied (*i.e.,* the repetition rate of the laser (R, in Hz) and the flow rate of the cells (F, in m/s) should be set such that the pixel size in the

flow direction is F/R <2**δ***y,* where **δ***y* is the diffraction-limited resolution along the flow direction). Note that the specifications of the grating (*e.g.,* groove density) and objective lens (*e.g.,* the numerical aperture (NA)) should be carefully designed to match the targeted resolution.

While the current ATOM demonstration and protocol show that the data acquisition is done by oscilloscope and the data processing is followed offline, it is more favorable to achieve real-time, continuous data acquisition, processing, and even analytics, especially leveraging the ability to achieve the ultrafast and high-contrast image capture abilities brought by ATOM. To this end, a high-performance and high-throughput signal processing unit should be adopted, such as a graphical processing unit (GPU) and/or a field-programmable gate array (FPGA), which have been demonstrated to have the capability to achieve a data processing throughput as high as ~1-10 GB/s. This is compatible with the ultrafast sampling ability of ATOM (*i.e.,* ~10 GSa/s). The integration of ATOM and a high-throughput data processing accelerator enables a new paradigm in data-driven biological studies, especially in unraveling the unknown heterogeneity between different single cells within an enormous population. Such technology could also empower a new generation of clinical research, in which rare, aberrant cells during the disease process can be quantified in a label-free manner.

Disclosures

The authors have nothing to disclose.

Acknowledgements

We thank Mr. P. Yeung for preparing the MCF-7 for us. This work was partially supported by grants from the Research Grant Council of the Hong Kong Special Administration Region, China (Project no. 17259316, 17207715, 17207714, 17205215, and HKU 720112E), the Innovation and Technology Support Programme (ITS/090/14), and the University Development Fund of HKU.

References

1. Lau, A.K.S., Wong, T.T.W., Shum, H.C., Wong, K.K.Y., & Tsia, K.K. In: *Imaging Flow Cytometry: Methods and Protocols.* Barteneva, N.S., & Vorobjev, I.A., eds., Springer New York, New York, NY, 23-45 (2016).
2. Goda, K., Tsia, K.K., & Jalali, B. Serial time-encoded amplified imaging for real-time observation of fast dynamic phenomena. *Nature.* **458** (7242), 1145-1149 (2009).
3. Goda, K., & Jalali, B. Dispersive Fourier transformation for fast continuous single-shot measurements. *Nat Photon.* **7** (2), 102-112 (2013).
4. Lau, A.K., Shum, H.C., Wong, K.K., & Tsia, K.K. Optofluidic time-stretch imaging - an emerging tool for high-throughput imaging flow cytometry. *Lab Chip.* **16** (10), 1743-1756 (2016).
5. Lau, A.K.S., Tang, A.H.L., J. Xu, X.W., Wong, K.K.Y., & Tsia, K.K. Optical Time Stretch for High-Speed and High-Throughput Imaging - From Single-Cell to Tissue-Wide Scales. *IEEE J. Sel. Top. in Quant. Electron.* **22** (2016).
6. Lei, C., Guo, B., Cheng, Z., & Goda, K. Optical time-stretch imaging: Principles and applications. *Appl Phys Rev.* **3** (1), 011102 (2016).
7. Lei, C., Guo, B., Cheng, Z., & Goda, K. Optical time-stretch imaging: Principles and applications. *Applied Physics Reviews.* **3**, 011102 (2016).
8. Goda, K. *et al.* High-throughput single-microparticle imaging flow analyzer. *Proc Natl Acad Sci U S A.* **109** (29), 11630-11635 (2012).
9. Goda, K., Solli, D.R., Tsia, K.K., & Jalali, B. Theory of amplified dispersive Fourier transformation. *Physical Review A.* **80** (4), 043821 (2009).
10. Goda, K. *et al.* High-throughput single-microparticle imaging flow analyzer. *Proc Natl Acad Sci U S A.* **109** (29), 11630-11635 (2012).
11. Lai, Q.T.K. *et al.* High-throughput time-stretch imaging flow cytometry for multi-class classification of phytoplankton. *Opt. Express.* **24** (25), 28170-28184 (2016).
12. Chen, C.L. *et al.* Deep Learning in Label-free Cell Classification. *Sci Rep.* **6**, 21471 (2016).
13. Fard, A.M. *et al.* Nomarski serial time-encoded amplified microscopy for high-speed contrast-enhanced imaging of transparent media. *Biomed Opt Express.* **2** (12), 3387-3392 (2011).
14. Lau, A.K. *et al.* Interferometric time-stretch microscopy for ultrafast quantitative cellular and tissue imaging at 1 mum. *J Biomed Opt.* **19** (7), 76001 (2014).
15. Mahjoubfar, A., Chen, C., Niazi, K.R., Rabizadeh, S., & Jalali, B. Label-free high-throughput cell screening in flow. *Biomed Opt Express.* **4** (9), 1618-1625 (2013).
16. Wong, T.T. *et al.* Asymmetric-detection time-stretch optical microscopy (ATOM) for ultrafast high-contrast cellular imaging in flow. *Sci Rep.* **4**, 3656 (2014).
17. Mata, T.M., Martins, A.A., & Caetano, N.S. Microalgae for biodiesel production and other applications: A review. *Renew Sustainable Energy Rev.* **14** (1), 217-232 (2010).
18. Irigoien, X., Huisman, J., & Harris, R.P. Global biodiversity patterns of marine phytoplankton and zooplankton. *Nature.* **429** (6994), 863-867 (2004).
19. Wei, X. *et al.* Coherent Laser Source for High Frame-Rate Optical Time-Stretch Microscopy at 1.0 µm. *IEEE J. Sel. Top. Quantum Electron.* **20** (5), 384-389 (2014).
20. Wei, X. *et al.* Breathing laser as an inertia-free swept source for high-quality ultrafast optical bioimaging. *Opt. Lett.* **39** (23), 6593-6596 (2014).
21. Xu, Y., Wei, X., Ren, Z., Wong, K.K.Y., & Tsia, K.K. Ultrafast measurements of optical spectral coherence by single-shot time-stretch interferometry. *Sci Rep.* **6**, 27937 (2016).
22. Tsia, K.K., Goda, K., Capewell, D., & Jalali, B. Performance of serial time-encoded amplified microscope. *Opt. Express.* **18** (10), 10016-10028 (2010).
23. Alix-Panabieres, C., & Pantel, K. Challenges in circulating tumour cell research. *Nat Rev Cancer.* **14** (9), 623-631 (2014).
24. Kling, J. Beyond counting tumor cells. *Nat Biotech.* **30** (7), 578-580 (2012).
25. Hodgkinson, C.L. *et al.* Tumorigenicity and genetic profiling of circulating tumor cells in small-cell lung cancer. *Nat Med.* **20** (8), 897-903 (2014).
26. Ozkumur, E. *et al.* Inertial focusing for tumor antigen-dependent and -independent sorting of rare circulating tumor cells. *Sci Transl Med.* **5** (179), 179ra147 (2013).

27. Hou, H.W. *et al.* Isolation and retrieval of circulating tumor cells using centrifugal forces. *Scientific Reports.* **3**, 1259 (2013).
28. Karabacak, N.M. *et al.* Microfluidic, marker-free isolation of circulating tumor cells from blood samples. *Nat. Protocols.* **9** (3), 694-710 (2014).
29. Krebs, M.G. *et al.* Molecular analysis of circulating tumour cells-biology and biomarkers. *Nat Rev Clin Oncol.* **11** (3), 129-144 (2014).
30. Wu, Jianglai. *et al.* Ultrafast Laser-Scanning Time-Stretch Imaging at Visible Wavelengths. *Light Sci Appl.* (2016).

